JOURNAL OF MATERIALS SCIENCE 23 (1988) 3771–3777

Sintering of hydroxylapatite–zirconia composite materials

JENN-MING WU, TUNG-SHENG YEH
Department of Materials Science and Engineering, National Tsing Hua University, Hsinchu, Taiwan 30043

Sintering of hydroxylapatite–zirconia (doped with 3 mol% Y_2O_3) composite powder compacts was studied. Hydroxylapatite powder was prepared from $Ca(OH)_2$ and H_3PO_4, and zirconia powder was prepared from $ZrOCl_2 \cdot 8H_2O$ and YCl_3. The sinterability of hydroxylapatite–zirconia composite powder compacts depends strongly on differential shrinkage between the powder components of the composite. Smaller differential shrinkage results in better sinterability. By increasing the calcination temperature of zirconia powder and/or decreasing that of hydroxylapatite powder improves the sinterability of the composite powder compacts. The phase distribution and total amounts of crystal phases depend on the sintered density of compacts. Hydroxylapatite and cubic zirconia are the major phases of compacts with high sintered densities, whereas α- and β-tricalcium phosphate and $CaZrO_3$ are the major phases of compacts with low sintered densities.

1. Introduction

Hydroxylapatite is a particularly attractive material for bone and tooth implants because its chemical and crystallographic properties closely resemble those of bone and tooth minerals, and the sintered material has superior compatibility with these tissues [1–3]. The principal limitation of this material is that it is brittle and weak [4–8], which restricts the clinical orthopaedic and dental applications. Zirconia, especially partially stabilized zirconia, has received special attention, primarily because of its high strength and high resistance to fracture [9–13]. Hulbert *et al.* [14] evaluated three different ceramics, $CaO \cdot Al_2O_3$, $CaO \cdot TiO_2$ and $CaO \cdot ZrO_2$, and concluded that they are inert bioceramics. The incorporation of ZrO_2 into hydroxylapatite material may enhance its mechanical properties and will not affect its biocompatibility. Thus it is desirable to study the hydroxylapatite–ZrO_2 composite materials. In the present paper sintering of hydroxylapatite and ZrO_2 composite materials is reported.

2. Experimental procedure

2.1. Preparation of hydroxylapatite powders

A suspension of 0.3 M $Ca(OH)_2$ in 1500 ml distilled water was vigorously stirred and its temperature was maintained at 70° C. A solution of 0.3 M H_3PO_4 in 1000 ml distilled water was slowly added dropwise to the $Ca(OH)_2$ suspension. The reaction mixture was stirred vigorously and aged for 24 h in a 70° C water bath. The resulting slurry was filtered, washed with deionized water three times, and washed with ethyl alcohol twice. The washed and filtered powder was dried and then calcined at 750 or 800° C for 3 h.

2.2. Preparation of ZrO_2 powders

Zirconia powders partially stabilized with 3 mol% Y_2O_3 were prepared by the oxychloride method. A suitable proportion of $ZrOCl_2 \cdot 8H_2O$ and YCl_3 was weighed and added to deionized water to form a solution of 0.3 M concentration. The solution was added slowly to an NH_4OH solution of pH = 9.35. To maintain the pH at 9.35, additional NH_4OH solution was added to the reaction solution simultaneously. After reaction, the turbid solution was filtered and washed with deionized water three times to remove chlorine ions. Then the filtered powder was washed with ethyl alcohol three times and dried. The resulting powder was calcined at various temperatures for 1 h.

2.3. Sintering of hydroxylapatite–zirconia composite

The calcined hydroxylapatite powder and zirconia powder were milled in a polyethylene bottle with zirconia balls for 10 h. The milling medium was ethyl alcohol. During ball milling, 1.5 wt % PVA was added as binder. The milled powder was then quickly filtered to prevent segregation due to the density difference of these two powders. In addition, the filtered powder cake was mixed in a pestle and mortar during drying. The resulting powder was then dry pressed at 100 MPa, and sintered at various temperatures for 3 h. The sintered bulk density was measured by Archimedes method. The crystal phases were identified using X-ray diffraction. The microstructure was investigated by scanning electron microscopy (SEM) on fractured and/or polished sample surfaces. For polished samples, the surface was etched with 0.1 M acetic acid or 1 wt % phosphoric acid before being investigated by SEM.

3. Results and discussion

3.1. Powder characteristics

Precipitated hydroxylapatite powder was dissolved by

0022–2461/88 $03.00 + .12

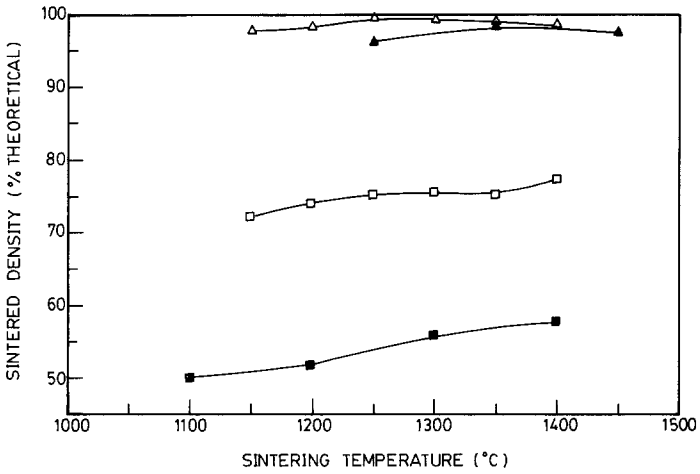

Figure 1 Sintered density plotted against sintering temperature for (△) hydroxylapatite (HAP), (▲) zirconia (Z5), and hydroxylapatite–zirconia composites (□, H8Z5 and ■, H0Z0).

nitric acid and then analysed by inductively coupled plasma-atomic emission spectroscopy (ICP–AES). The calcium/phosphorus molar ratio was determined to be 1.66 + 0.01, very close to the theoretical ratio for hydroxylapatite, i.e. 1.667. The major impurity of the precipitated hydroxylapatite was manganese, the concentration of which was determined to be 100 p.p.m. The crystal phase of precipitated hydroxylapatite powder before calcination and after calcining at 750 and 800° C for 3 h was all hydroxylapatite. The observed X-ray peaks were broad. The precipitated hydroxylapatite powder was needle-shaped approximately 100 nm long and 20 nm wide, as observed by TEM before calcination. After calcination, powder growth occurs as evidence of sharper X-ray diffraction and direct TEM images. Powders calcined at 750 and 800° C for 3 h were approximately 160 nm long, 30 to 40 nm wide, and 190 nm long, 40 nm wide, respectively. The surface areas measured by the BET method were 35.0 and 32.1 $m^2 g^{-1}$, respectively, for 750 and 800° C calcination. The bulk density sintered at various temperatures for the 800° C calcined powder was shown in Fig. 1. The powder compact can be sintered to high density in the temperature range 1150 to 1350° C, 97% theoretical density at 1150° C, and 99.5% theoretical density at 1300° C. The crystal phase of the sintered sample was determined to be hydroxylapatite no other phases were observed. These demonstrate the excellent sinterability and high stability of the precipitated hydroxylapatite powder.

The precipitated zirconia powder is amorphous before calcination, and shows tetragonal structure after calcining at temperatures higher than 550° C for 1 h. The crystallite shape is spherical. The crystallite size is about 10 to 20 nm for calcining at temperatures from 550 to 800° C, and 0.1 μm for 1200° C calcination. The bulk densities sintered for 3 h at various temperatures for precipitated zirconia powder calcined at 550° C for 1 h are shown in Fig. 1, demonstrating that the calcined zirconia powder compact can also be sintered easily to high density, about 95% to 98% theoretical. The crystal phase of the fired compact is single-phase tetragonal zirconia.

3.2. Sintering of hydroxylapatite–ZrO_2 composite (H8Z5)

Fig. 1 also shows the sintered densities of powder compacts which consist of 80 wt % hydroxylapatite powder calcined at 800° C for 3 h and 20 wt % ZrO_2 powder calcined at 550° C for 1 h (H8Z5). The sintered bulk densities are estimated to be about 70 to 80% theoretical density assuming no phase reaction. From X-ray diffraction, it is found that phase transformation and reaction occur extensively as the sintering temperature increases. Fig. 2 shows the X-ray diffraction peaks for samples sintered at different temperatures and then ground into powder. The range of 2θ is shown from 29° to 34° where the phase change can be easily differentiated. At 1150° C, some hydroxylapatite phase has transformed into β-tricalcium phosphate (whitlockite), and tetragonal zirconia has transformed into cubic zirconia. In addition, the released CaO, due to transformation of hydroxylapatite into β-tricalcium phosphate, reacted with ZrO_2 to form $CaZrO_3$. As the sintering temperature increases, the amounts of β-tricalcium phosphate

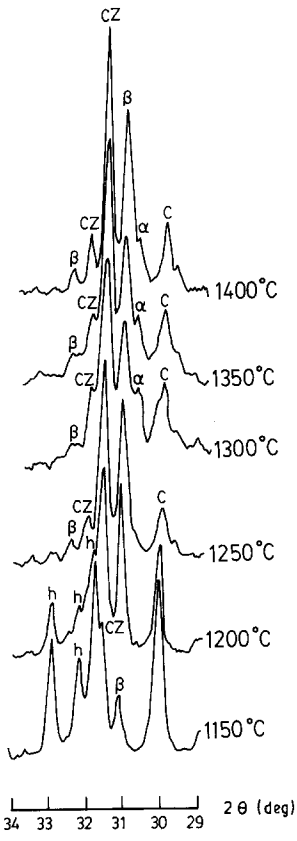

Figure 2 Crystal phases of hydroxylapatite–zirconia composites after sintering at various temperatures from 1150 to 1400° C. $\alpha = \alpha$-C_3P; $\beta = \beta$-C_3P; C = cubic ZrO_2; h = HAP; CZ = $CaZrO_3$.

and $CaZrO_3$ phase continue to increase, and those of hydroxylapatite and cubic ZrO_2 tend to decrease. At 1400° C, almost no hydroxylapatite phase is left. Some β-tricalcium phosphate has transformed into α-tricalcium phosphate. However, even if the density changes caused by phase transformation and reaction are considered, the sintered bulk densities increase only about 3% on the theoretical density scale, i.e. lie between 73 to 83% theoretical.

The sinterability of the composite is very poor compared with the original individual powders. Fig. 3 shows the microstructures of fracture surfaces of the composite sintered at different temperatures. There is significant agglomeration of ZrO_2 powders which are shown as small spherical particles in Fig. 3a. The small spherical particles were identified as ZrO_2 powders partly from TEM powder images and partly from electron probe microanalysis (EPMA). The pores are connective in all sintered compacts. By comparing Figs 3a to f, it is found that pore (or open channel) size tend to grow as sintering temperature increases. From X-ray diffraction data, the connective phases are either hydroxylapatite or tricalcium phosphate, and the dispersed phases are either cubic ZrO_2 or $CaZrO_3$ phase. The poor sinterability of the composite powder compact apparently resulted from extensive pore development during sintering. This pore development or fissure formation may be caused either by water vapour evolution due to reaction between hydroxylapatite and zirconia or by differential shrinkage of the individual powder. It is felt that differential shrinkage is the major factor affecting the sintering behaviour of the powder composite because of different packing of these two powders. Applying 100 MPa consolidation pressure to individual powders, the green densities of the compacts are found to be about 30% and 50% theoretical density for zirconia and hydroxylapatite powder, respectively. Assuming both powders are sintered to full density, the average linear shinkage should be 33% for zirconia powder, and 20.6% for hydroxylapatite. The shrinkage of zirconia powder is larger by (33–20.6)/20.6 = 60% than that of hydroxylapatite powder. This tremendous shrinkage difference detaches zirconia agglomerate from the hydroxylapatite matrix and forms extensive pores or fissures which are difficult to eliminate as sintering proceeds.

3.3. Effect of calcination on sintering (H0Z0, H8Z8, H8Z12, H7Z12)

Because the poor sinterability of hydroxylapatite–zirconia powder composite was hypothesized to result from differential shrinkage between hydroxylapatite matrix and zirconia agglomerates, it is thought that the sinterability can be improved if the agglomerate can be reduced. In order to achieve more intimate mixing of hydroxylapatite and zirconia powders, the two powders were mixed after they were precipitated and before they were calcined. The suspensions of hydroxylapatite and zirconia precipitates were prepared by the methods mentioned in the previous section; however, the zirconia precipitate suspension was added dropwise to the hydroxylapatite precipitate suspension before they were filtered. During this step, both suspensions were stirred vigorously to achieve intimate mixing and to prevent segregation. As the procedure was completed, the whole suspension was filtered and washed with water and ethyl alcohol as before. The powder prepared this way was represented as H0Z0. The sintered densities were shown in Fig. 1. The sinterability of H0Z0 powder was even worse than that of H8Z5. From microstructural investigations, which are similar to Fig. 3 and will not be shown here, it was found that although the agglomerate size seemed reduced, the agglomeration could not be eliminated. Thus it is reasoned that the poorer sinterability may arise from the looser packing of both powders which results in larger differential shrinkage.

Another approach to reduce the differential shrinkage is reducing the shrinkage of zirconia and/or increasing that of hydroxylapatite. Based on this argument, zirconia powders were calcined at 800° C (Z8) and 1200° C (Z12) for 1 h (previously at 550° C (Z5)). The effect of calcination on sintering is demonstrated in Fig. 4. Comparing the sintered densities of H8Z12, H8Z8 (Fig. 4), and H8Z5 (Fig. 1), it is found that the increase of calcination temperature from 550 to 800° C changes the sintered densities very little, whereas increasing the calcination temperature from 800 to 1200° C increases sintered densities very significantly. This may be due to the small change in crystallite size from 550 to 800° C and the large increase in crystallite size from 800 to 1200° C, mentioned in the previous section. Increasing the calcination temperature of zirconia powder causes zirconia particles to grow and the packing density of the zirconia agglomerate to increase. This reduces the shrinkage of the zirconia agglomerate and thus the differential shrinkage between hydroxylapatite and zirconia. Slower formation of pores and fissures enhances sintering. Comparing H7Z12 and H8Z12 in Fig. 4, it is demonstrated that reducing the calcination temperature of hydroxylapatite powder tends to improve the sinterability of the composite even further. H7Z12 represents samples in which the hydroxylapatite powder was calcined at 750° C for 3 h and the zirconia powder was calcined at 1200° C for 1 h. Reducing the calcination temperature of hydroxylapatite powder has the effect of decreasing the particle size and particle packing density of hydroxylapatite. This increases the shinkage of hydroxylapatite during sintering and makes the differential shrinkage smaller, which helps sintering. The sintered densities of H7Z12 composite are very close to the theoretical density of the composite.

The change in crystal phase during sintering of all the composites consisting of hydroxylapatite and zirconia has a similar trend. As sintering temperature increases, hydroxylapatite tends to release CaO and transform into β-tricalcium phosphate, and zirconia tends to react with released CaO and form cubic zirconia of $CaZrO_3$. The higher the sintering temperature, the larger the amounts of β-tricalcium phosphate and $CaZrO_3$. As temperature increases further, β-tricalcium phosphate transforms into α-tricalcium phosphate. Although the tendency of the phase change with sintering temperature is similar for all

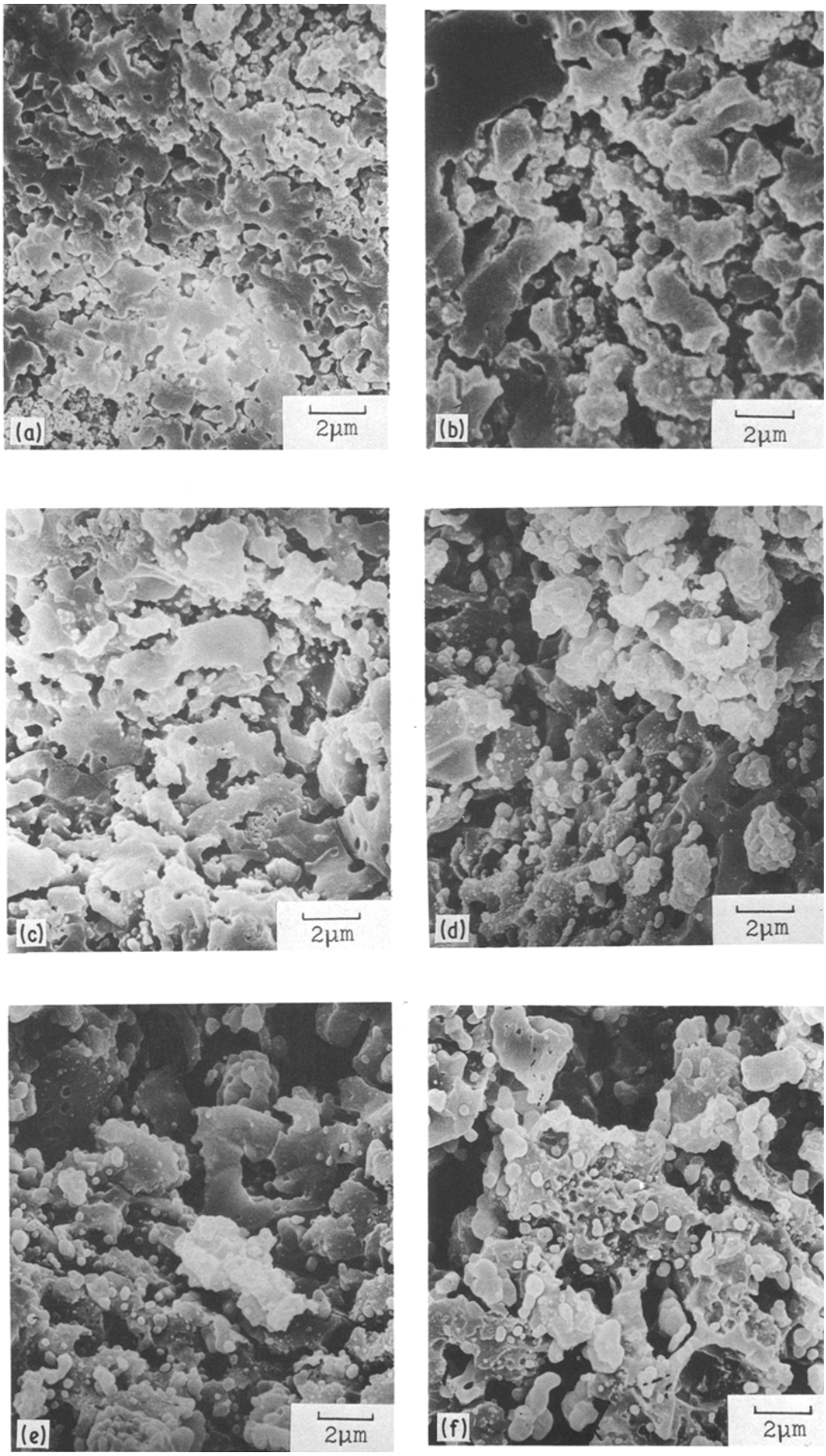

Figure 3 Microstructures of fracture surfaces of hydroxylapatite–zirconia composite (H8Z5) sintered at various temperatures: (a) 1150° C; (b) 1200° C; (c) 1250° C; (d) 1300° C; (e) 1350° C; (f) 1400° C.

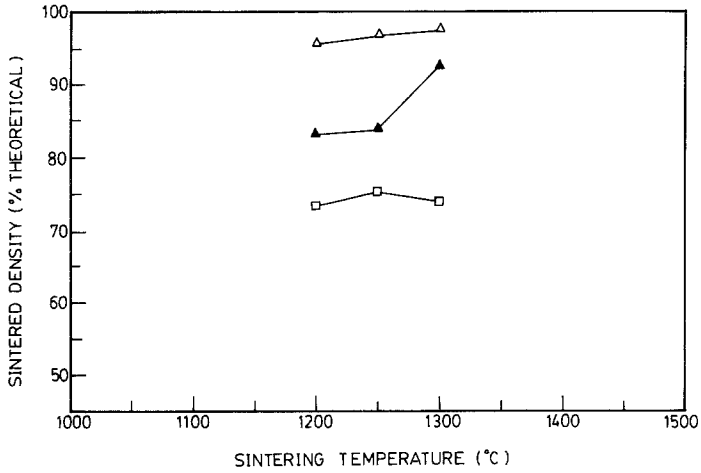

Figure 4 Sintered density plotted against sintering temperature for hydroxylapatite–zirconia composites (□) H8Z8, (▲) H8Z12, (△) H7Z12.

composite powder compacts, the total amounts and distribution of tricalcium phosphates and $CaZrO_3$, which depend on the sintered density of compact, differ greatly.

3.4. Phase distribution of sintered hydroxylapatite–zirconia composite

The phase distribution from the surface to the centre of the sintered compact can be obtained by polishing the sample to the desired depth and analysing the crystal phases of the sample surface with X-ray diffraction. Fig. 5a is a schematic diagram showing the relative distribution of the phosphate phases of the composite which cannot be sintered to high density. The hydroxylapatite transforms into α- and β-tricalcium phosphate within the whole sample. Samples which show this kind of distribution include composites H8Z8 which were sintered at 1200, 1250 and 1300° C as well as composites H8Z12 which were sintered at 1200 and 1250° C (Fig. 4). Fig. 5b is a schematic diagram showing the relative distribution of phosphate phases of the composites which can be sintered to nearly theoretical density. The transformation of hydroxylapatite into α- and β-tricalcium phosphate is limited to the surface layer with a thickness of about 100 to 200 μm, depending on sintered density and sintering temperature. In addition, the distribution of tricalcium phosphate phases is not uniform in the surface layer: α-tricalcium phosphate accumulates on the outer surface region, whereas β-tricalcium phosphate tends to locate on the inner surface region. Samples which show this kind of

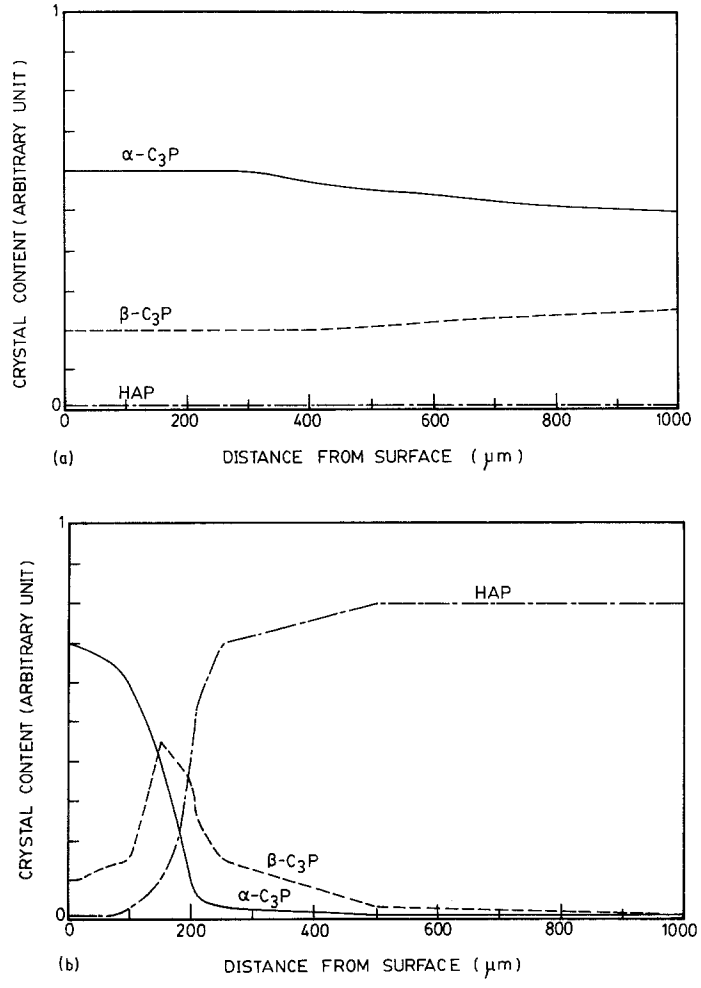

Figure 5 Variation of crystal phases with distance from as-sintered surface for composites with (a) low sintered density, and (b) high sintered density.

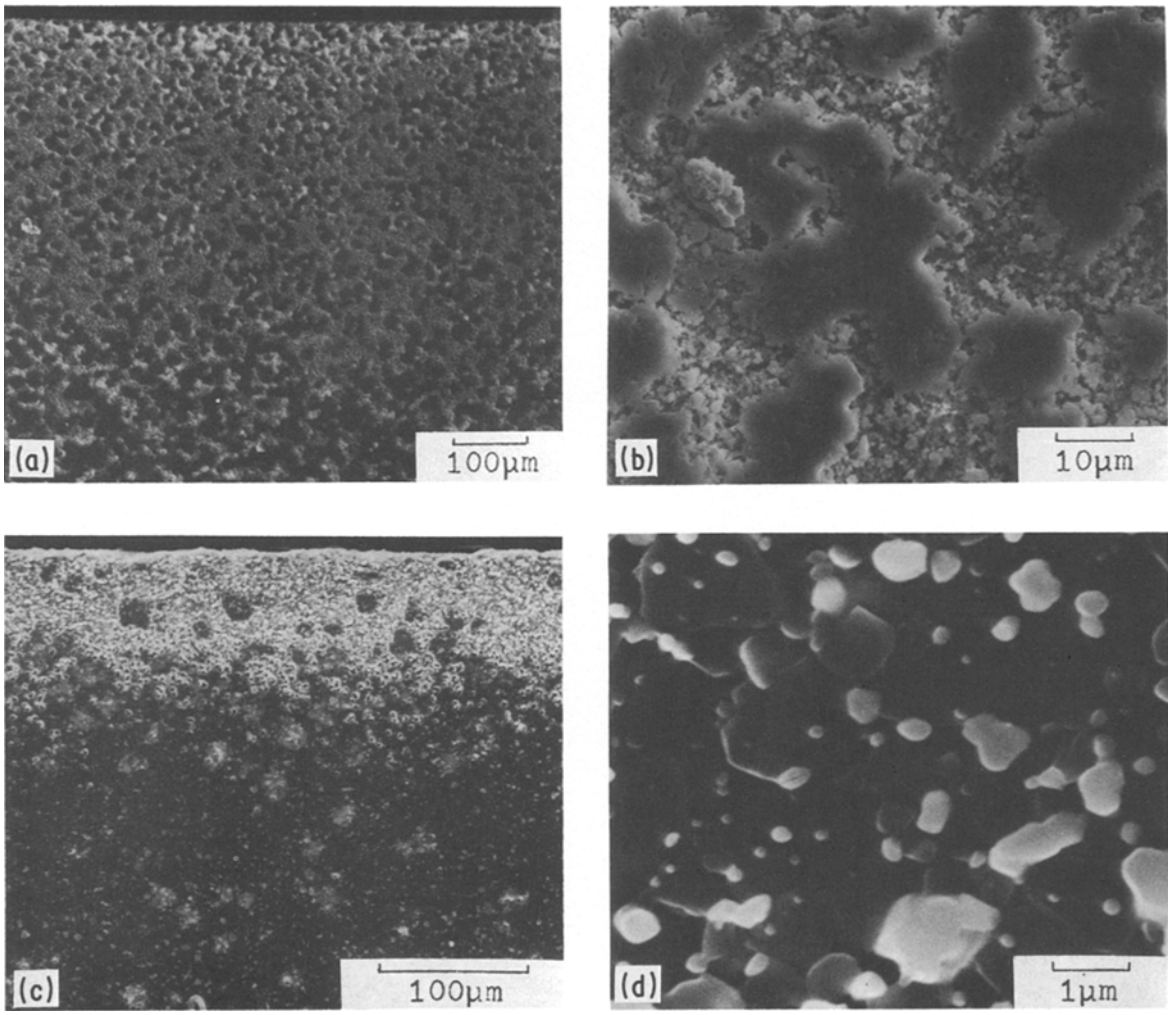

Figure 6 Microstructures of cross-sections of two typical samples which have low sintered densities, (a) surface region, (b) centre; and high sintered densities (c) surface region, (d) centre.

distribution include composites H7Z12 which were sintered at 1200, 1250, and 1300° C, as well as composite H8Z12 which was sintered at 1300° C.

The phase distribution obtained by X-ray diffraction is consistent with the observed microstructures. Fig. 6a is an SEM picture of the cross-section of sample H8Z12 sintered at 1200° C for 3 h, polished and etched in 0.1 M acetic acid solution for 1 min. The sample surface is located near the top of the picture. Two types of regions can be differentiated from the microstructure. One is the white area which covers most of the microstructure, appearing densely interconnected in the outer surface region and less densely distributed on approaching the centre of the sample. The other is the dark region which is isolately distributed in the outer surface region. The area of the dark region increases on approaching the centre of the sample, and its distribution becomes interconnected. Fig. 6b exhibits the microstructure of the centre of the same sample as Fig. 6a, showing that the dark area is larger than the white area; the white area is actually the area where crystals are more easily etched away, and the dark area is the area where crystals have a higher resistance to acid corrosion. As compared to X-ray diffraction data, it is concluded that the white area is α-tricalcium phosphate, and the dark area is β-tricalcium phosphate. The cubic-zirconia and $CaZrO_3$ phases are embedded in the phosphate phases. Fig. 6c shows the microstructure of the cross-section of H7Z12 sintered at 1300° C for 3 h. Fig. 6c shows the same characteristics as Fig. 6a, the major differences between them being: the white area is more densely distributed in the outer surface; the white area is much thinner, approximately 100 μm thick; the white area is isolately and sporadically distributed within a 100 to 1000 μm region from the surface. The microstructure of the centre of this sample is shown in Fig. 6d, being composed of dark matrix grains with diameters of approximately 1 μm and white particles of size varying from 0.1 to 0.5 μm. On comparison with X-ray diffraction data and microstructures of sintered pure hydroxylapatite compact, the dark matrix grain is identified as hydroxylapatite phase and the white particle is essentially cubic zirconia phase. The microstructures of other samples are either similar to Figs 6a and b or similar to Figs 6c and d. Compacts which can be sintered to high density, i.e. H7Z12 sintered at 1200, 1250, and 1300° C and H8Z12 sintered at 1300° C, all possess the same microstructures as Figs 6c and d. Compacts which have low sintered densities, on the other hand, such as H8Z12 sintered at 1200 and 1250° C, and H8Z8 sintered at 1200, 1250 and 1300° C, show the same microstructures as Figs 6a and b.

The phase distribution and total amounts of crystal phases apparently depend on the sintered density. This can be explained by the following reactions

$$Ca_{10}(PO_4)_6(OH)_2 \rightleftharpoons 3\beta\text{–}Ca_3P_2O_8 + CaO + H_2O \quad (1)$$

$$CaO + ZrO_2 \rightleftharpoons \text{cubic-}ZrO_2 \text{ or } CaZrO_3 \quad (2)$$

$$\beta\text{–}Ca_3P_2O_8 \rightleftharpoons \alpha\text{–}Ca_3P_2O_8 \quad (3)$$

From Reaction 1, hydroxylapatite transforms into β-tricalcium phosphate together with releasing calcium (or CaO) and evolving water vapour. If the composite compacts cannot be sintered to high density, water vapour can diffuse out of the sample easily through interconnected open pores, Reaction 1 tends to move to the right. Hydroxylapatite phase is not stable, and α- or β-tricalcium phosphate are the major phases. According to Reaction 1, the reaction continues, a lot of CaO is released, thus $CaZrO_3$ is formed in preference to cubic zirconia. If the compacts can be sintered to nearly theoretical density, the water vapour evolved according to Reaction 1 has little opportunity to diffuse out of the sample, except in the region which is close to the surface. Thus hydroxylapatite is stable in the most part of the sample except the surface layer, and α- as well as β-tricalcium phosphate are the main phases in the surface layer. Because the amount of released CaO is small in the region which is away from the surface layer, cubic zirconia is the major zirconia-containing phase. The thickness of the surface layer depends strongly on the ease of the diffusion of water vapour which is closely related to the sintered density. The higher the sintered density, the thinner the surface layer.

4. Conclusion

The sinterability of hydroxylapatite–zirconia composite powder compacts depends greatly on differential shrinkage between the powder components of the composite. The smaller the differential shrinkage, the better the sinterability of the composite powder compact. Because the shrinkage of zirconia agglomerate is higher than that of hydroxylapatite for powders prepared in this study, treatments such as calcining zirconia powder at higher temperature and calcining hydroxylapatite powder at lower temperature, improve the sinterability of the composite powder compact.

The phase distribution and total amounts of crystal phases depend on the sinterability of composite powder compacts. For compacts which can be sintered to nearly theoretical density, the evolved water vapour cannot diffuse out of the sample fast enough for hydroxylapatite and cubic zirconia to be the major phases in the most part of the sample except in the surface layer where α- and β- tricalcium phosphates and $CaZrO_3$ are the major phases. For compacts which have low sintered density, water vapour can diffuse easily through interconnected open pores, α- and β-tricalcium phosphate and $CaZrO_3$ are the major phases in the whole sample.

References

1. E. B. NERY, K. L. LYNCH, W. M. HIRTHE and K. H. MUELLER, *J. Periodontol.* **46** (1975) 328.
2. M. JARCHO, K. I. GUMAER, J. F. KAY, R. H. DOREMUS and H. P. DROBECK, *J. Bioeng.* **1** (1977) 79.
3. H. AOKI, K. KATO and T. TABATA, *Rep. Inst. Med. Dent. Eng. Jpn* **11** (1977) 33.
4. W. R. RAO and R. F. BOEHM, *J. Dent. Res.* **53** (1974) 1351.
5. M. JARCHO, C. H. BOLEN, M. B. THOMAS, J. BOBICK, J. F. KAY and R. H. DOREMUS, *J. Mater. Sci.* **11** (1976) 2027.
6. W. VAN RAEMDONCK, P. DUCHEYNE and P. DE MEESTER, in "Metal and Ceramic biomaterials", CRC Press Inc, Florida, (1984) Vol II, p. 143.
7. K. DE GROOT, in "Bioceramics of Calcium Phosphate" (CRC, Florida, 1983) p. 102.
8. G. DE WITH, H. J. A. VAN DIJCK, N. HATTU and K. PRIJS, *J. Mater. Sci.* **16** (1981) 1592.
9. R. S. GARVIE, R. H. J. HANNINK and R. T. PASCOE, *Nature* **258** (1975) 703.
10. D. L. PORTER and A. H. HEUER, *J. Amer. Ceram. Soc.* **60** (1977) 183.
11. F. F. LANGE, *J. Mater. Sci.* **17** (1982) 247.
12. *Idem, ibid.* **17** (1982) 255.
13. N. CLAUSSEN and M. RUHLE, in "Advances in Ceramics", Vol. 4, "Science and Technology of Zirconia" (American Ceramic Society, Columbus, Ohio, 1981) p. 339.
14. S. F. HULBERT, J. S. MORRISON and J. J. KLAWITTER, *J. Biomed. Mater. Res.* **6** (1972) 347.

Received 16 September 1987
and accepted 19 January 1988